

DOI:10.1002/ejic.201300849

Strongly Blue Luminescent Cationic Iridium(III) Complexes with an Electron-Rich Ancillary Ligand: Evaluation of Their Optoelectronic and Electrochemiluminescence Properties

Sébastien Ladouceur,^[a] Kalen N. Swanick,^[b]
Shawn Gallagher-Duval,^[a] Zhifeng Ding,^{*[b]} and
Eli Zysman-Colman^{*[a,c]}

Keywords: Iridium / Electrochemistry / Nitrogen heterocycles / UV/Vis spectroscopy / Electrochemiluminescence / Density functional calculations

Two strongly blue luminescent cationic heteroleptic iridium complexes **1b** and **2b** bearing a 4,4'-bis(dimethylamino)-2,2'-bipyridine (dmabpy) ancillary ligand and either 1-benzyl-4-(2,4-difluorophenyl)-1*H*-1,2,3-triazole (dFphtl) or 2-(2,4-difluorophenyl)-5-methylpyridine (dFMepyH), respectively, have been synthesized and fully characterized. In comparison with other analogues, the interplay of the triazole unit with the dmabpy unit and methylation of the pyridine ring are discussed with respect to the photophysical, electrochemical, and electrochemiluminescent (ECL) properties of the complexes. The two complexes, **1b** and **2b**, are blue emitters with $\lambda_{\text{max}} = 495$ and 494 nm, respectively. The nature of the excited states was established by various photophysical and photochemical experiments as well as DFT calculations. Both complexes emit from a ligand-centered state, however, the emission of **1b** possesses significant charge-transfer character, which is absent in **2b**. The presence of the methyl group


on the cyclometalating ligand leads only to a modest increase in the radiative rate constant, k_r , but otherwise does not appreciably influence the optoelectronic properties of the complex compared with the non-methylated analogue. In contrast, the efficacy of the ECL emission when scanning to 2.50 V is strongly influenced by the presence of the methyl group. ECL emission is also enhanced in complexes bearing dmabpy ancillary ligands compared with those containing dFbupy ligands. The two complexes exhibit similar electrochemical behavior. Incorporation of the dmabpy ligand shifts both the oxidation and reduction cathodically. The combination of the dmabpy and dFphtl groups increases the redox potential difference and thus the HOMO–LUMO gap but the emission is not further blueshifted. Thus, the structural modification of the cyclometalating ligand, although only modestly tuning the emission energy, modulates the nature of the excited state and the efficiency of the ECL process.

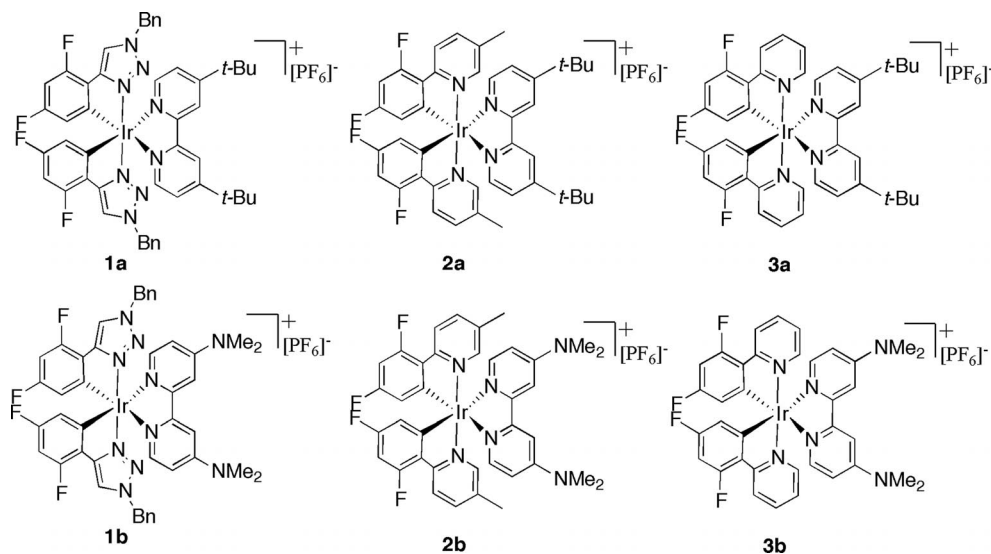
Introduction

Cationic iridium(III) complexes have come to the fore as the emissive molecules of first choice in diverse solid- and solution-state applications, such as light-emitting electrochemical cells (LEECs)^[1] and biological and environmental probes,^[2] owing to their attractive photophysical and physicochemical profiles, namely high quantum efficiencies, large window of accessible excited state lifetimes, a

HOMO–LUMO gap that is easily modulated, and great thermal and chemical stabilities. In particular, the integration of readily soluble Ir complexes with electrogenerated chemiluminescence (ECL) techniques will produce ECL-based assays with increased sensitivity compared with benchmark $[\text{Ru}(\text{bpy})_3]^{2+}$ derivatives with important implications for diverse biological and materials applications.^[3] Of late, there has been an increased number of reports on ECL behavior in both aqueous and nonaqueous media using both neutral^[4] and charged^[4e,4n,5] mononuclear, oligonuclear,^[6] and polymer-bound^[7] iridium(III) complexes. LEECs and ECL share a common mechanistic lineage as the generation of light from both applications results from the recombination of holes (radical cations) and electrons (radical anions), which were electrochemically generated to form excitons that relax radiatively back to the ground state.

For most applications, including full-color lighting and visual displays, access to a blue emitter is a prerequisite, and one that is phosphorescent is potentially advantageous.

- [a] Département de Chimie, Université de Sherbrooke, 2500 Blv. de l'Université, Sherbrooke, QC, Canada, J1K 2R1
[b] Department of Chemistry, The University of Western Ontario, 1151 Richmond Street, London, ON, Canada N6A 5B7
E-mail: zfding@uwo.ca
<http://publish.uwo.ca/~zfding/>
[c] School of Chemistry, University of St Andrews, St Andrews, Fife, KY16 9ST, UK
E-mail: ezc@st-andrews.ac.uk
<http://www.zysman-colman.com>
-  Supporting information for this article is available on the WWW under <http://dx.doi.org/10.1002/ejic.201300849>.

Scheme 1. Complexes **1a–3a** and **1b–3b** in this study.

For example, power consumption in organic light-emitting diodes (OLEDs) can be measurably improved with integrated phosphors in comparison with blue fluorophores.^[8] Through judicious modification of the ligand sphere, iridium complexes phosphorescing from red to sky-blue have been reported. However, highly luminescent blue luminophores are still missing. To the best of our knowledge, the “bluest” cationic iridium luminophores generally show structured ligand-centered (³LC) emission bands between 451–490 nm in either DCM (dichloromethane) or ACN (acetonitrile) solution, with photoluminescent quantum yield, Φ_{PL} , ranging from 3 to 54%;^[9] cationic iridium complexes incorporating σ -donating phosphane ancillary ligands demonstrate Φ_{PL} values as high as 80%.^[9i,10]

We^[11] and others^[12] have recently reported the use of aryltriazoles (atI) as cyclometalating ligands (C^N) for cationic iridium complexes of the form [(C^N)₂Ir(L^L)]⁺, in which L^L is a datively coordinating ligand such as 2,2'-bipyridine. We demonstrated that the replacement of a 2-phenylpyridine (ppy) C^N ligand by an atI resulted in a net blueshift (ca. 533 cm⁻¹) in the emission spectrum with an increase in quantum efficiency due in part to the presence of *N*-benzyl groups on the triazoles.^[11] The bluest of the emitters reported in our initial study, **1a** (Scheme 1), exhibits an emission λ_{max} of 499 nm in ACN solution at 298 K with $\Phi_{\text{PL}} = 80\%$, similar to a structurally related complex observed by De Cola and co-workers.^[12a] In addition, De Angelis et al.^[13] reported that the combined effects of electron-releasing substituents on the bipyridine ligand and of electron-withdrawing substituents on the phenylpyridine ligands can tune the emission to higher energy. Based on all the above, we hypothesized that substitution of the *dtBubpy* L^L ligand (*dtBubpy*: 4,4'-di-*tert*-butyl-2,2'-bipyridine) of **1a** by the more electron-donating *dmabpy* [*dmabpy*: 4,4'-bis(dimethylamino)-2,2'-bipyridine], as in **1b**, would produce the desired further blueshift. To assess the impact of the proposed structural modification on the pho-

tophysical behavior, we contrast **1b** with benchmark complex **2b**, a methylated analogue of **3b**, also known as N969.^[13b] We also explore the impact of methylation at the 5-position of the pyridine ring of the C^N ligand by a comparison between **2a** and **3a** and also between **2b** and **3b**, **3a** being a green-blue emitter previously reported by Bolink et al.^[14] Herein we report the solution-state photophysical and electrochemical behavior at ambient temperature along with photophysical data at 77 K for **1b** and **2b** and make comparisons with benchmark complexes **1a–3a** and **3b**. We also evaluate in a rational manner the ECL properties of **1b–3b** in order to discern the structure–property relationships relevant to the development of ECL luminophores. DFT calculations were also used to rationalize the structure–property relationships observed experimentally in our optoelectronic studies.

Results and Discussion

Synthesis

The ligand *dmabpy* was prepared in five steps in 12% overall yield following a much-improved synthetic procedure to that previously reported.^[15] Details of our higher-yielding synthesis of *dmabpy* may be found in the Supporting Information. Complexes **1b–3b** were synthesized in good yields by cleavage of the corresponding [(C^N)₂IrCl]₂ dimer with *dmabpy* in 2-EtOCH₂CH₂OH at reflux and anion metathesis with NH₄PF₆ following a modified procedure of Nonoyama.^[16] Similarly, **2a** and **3a** were obtained in good yields by cleavage of the corresponding [(C^N)₂IrCl]₂ dimer with *dtBubpy*. The complexes were characterized by their melting points, ¹H and ¹³C NMR spectroscopy, and low- and high-resolution MS, all of which provided satisfactory microanalysis.

Absorption Spectroscopy

The main spectroscopic and photophysical features of **1a–3a** and **1b–3b** are summarized in Tables 1 and 2 and Tables S1 and S2 in the Supporting Information. The absorption profiles of the six complexes are similar (see Figures S7 and S8), with intense bands above 300 nm that have been assigned to ligand-centered ¹LC π - π^* transitions. Moderate intensity bands in the range 350–450 nm have been assigned to metal–ligand/ligand–ligand charge-transfer (¹MLCT/¹LLCT) transitions. These CT bands are more intense for the dmabpy-containing complexes than those containing d/Bubpy due to the enhanced conjugation imparted by the NMe₂ groups. The absorption band at around 350 nm for **1b–3b** results from an ILCT transition mixed with some LC and MLCT character all involving the dmabpy ligand. This assignment is supported by time-dependent (TD) DFT calculations (see below). The increased intensity of this band was also observed in the case of [(dFppz)₂Ir(dmabpy)](PF₆) and was attributed to the enlarged π system of the dmabpy ligand [HdFppz = 1-(2,4-difluorophenyl)-1*H*-pyrazole].^[17] In addition, the strongly electron-donating dmabpy induces a redshift in the ¹LC bands of **1b** at 260 and 290 nm as well as in the MLCT and ¹LLCT bands at 349 nm compared with **1a**. The molar absorptivities of the absorption bands for **1b** are lower in CHCl₃ solution (see Table S1). The absorption profiles for

2b and **3b** in both ACN and CHCl₃ are similar to those of **1b**, although their bands are slightly bathochromically shifted and less intense.

Emission Spectroscopy

The photoluminescent spectra in ACN solution at 298 K for **1a–3a** and **1b–3b** are shown in Figure 1 (a) and those in a 1:1 MeOH/EtOH glass at 77 K are shown in Figure 1 (b) (emission spectra and photophysical data in CHCl₃ are found in Figures S8 and S9 and Table S2). Complexes **1a–3a** all exhibit unstructured emission with maxima at 498, 512, and 519 nm, respectively, characteristic of complexes emitting from a predominantly CT state. Incorporation of the methyl group into **2a** results in a small blueshift in the emission spectrum compared with **3a**, and replacement of the pyridine ring with a triazole in **1a** promotes a further blueshift. Complex **1b** also exhibits unstructured emission with a λ_{max} of 495 nm, however, both **2b** and **3b** show structured emission with emission maxima at 494 and 490 nm, respectively, and high-energy shoulders at 466 and 464 nm, respectively. The emission profile for **1b** is notable as most blue Ir luminophores such as **2b** show structured emission from a LC state that results in reduced color purity.^[9h] The λ_{max} for **1b** is blueshifted in CHCl₃ by 494 cm⁻¹ whereas no solvatochromism is observed for **2b** or **3b**. The difference in the emission profile between **1b** and **2b** (and **3b**) suggests a decrease in the ³CT character of the emission to one that is mainly ³LC in the last two complexes. Notable also is the absence of a further blueshift in the emission of **1b** compared with **1a**, unlike the expected blueshift observed with **2b** and **3b** compared with **2a** and **3a**. However, the same behavior was noted in ACN when comparing [(dFppz)₂Ir(dmabpy)](PF₆) ($\lambda_{\text{em}} = 493$ nm)^[17] with [(dFppz)₂Ir-(d/Bubpy)](PF₆) ($\lambda_{\text{em}} = 495$ nm).^[9g]

Table 1. Absorption data for **1a,b** and **2a,b** in aerated ACN at 298 K.

	λ_{abs} [nm] (ϵ [10^4 M ⁻¹ cm ⁻¹])
1a	215 (7.63), 235 (5.78), 300 (1.84), 375 (0.10)
1b	227 (7.19), 260 (6.81), 290 (4.44), 349 (0.97)
2a	250 (5.60), 295 (2.73), 360 (0.64), 420 (0.09)
2b	265 (6.99), 300 (3.69), 355 (1.26), 455 (0.03)

Table 2. Photophysical and spectroscopic for **1a,b** and **2a,b** in ACN solution.

	77 K ^[a,b]		λ_{em} [nm] 298 K ^[b] CH ₃ CN	298 K ^[b] CHCl ₃	Φ_{PL} [%] ^[c]		τ_{e} [μ s]		k_{r} [10^5 s ⁻¹]	k_{nr} [10^5 s ⁻¹]
	N ₂	Air			77 K ^[a]	298 K				
1a ^[d]	433 [0.85], 463 [1.00], 497 [0.74], 530 [0.38], 575[0.13]	498 [1.00]	491 [1.00]	74	4.9	4.26	1.20	6.1	2.2	
1b	459 [1.00], 488 [0.99], 521 [0.60], 560 [0.51], 615 [0.18]	495 [1.00]	487 [1.00]	47	0.4	11.8	6.18	0.8	0.9	
2a	456 [1.00], 488 [0.65], 511 [0.25]	512 [1.00]	521 [1.00]	76	3.7	6.48	1.19	6.4	2.0	
2b	459 [1.00], 492 [0.80], 525 [0.37]	466 [0.92], 494 [1.00], 525 [0.63]	464 [1.00], 495 [0.96], 525 [0.54]	74	0.6	4.66	3.13	2.3	0.8	

[a] Measured in 1:1 MeOH/EtOH glass. [b] Relative intensities are given in brackets. [c] Measured at 298 K by using quinine sulfate in 0.5 M H₂SO₄ ($\Phi = 55\%$)^[18] and [Ru(bpy)₃](PF₆)₂ as a second standard ($\Phi = 9.5$ and 1.8% in deaerated and aerated ACN, respectively).^[19] [d] Data taken from ref.^[11]

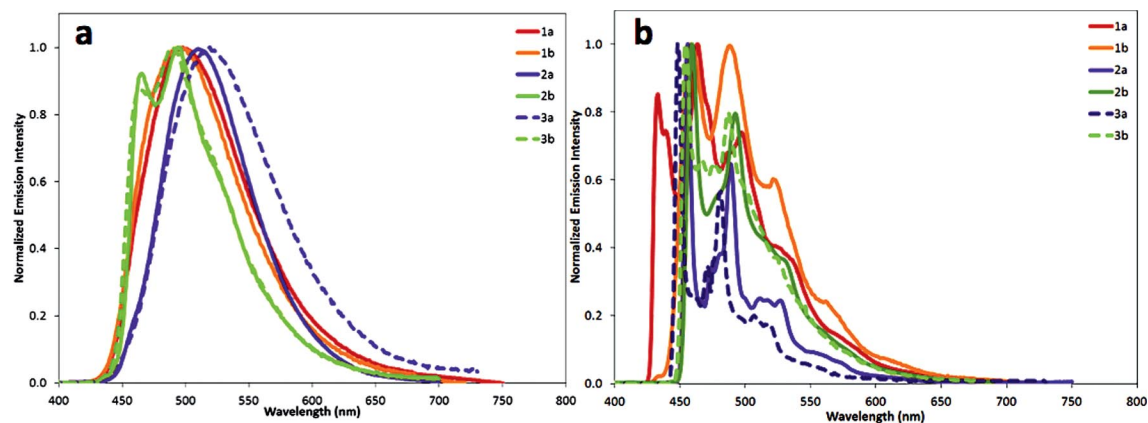


Figure 1. a) Emission spectra for **1a–3a** and **1b–3b** obtained in deaerated ACN solution at 298 K; b) emission spectra for **1a–3a** and **1b–3b** obtained in a 1:1 EtOH/MeOH glass at 77 K.

Complexes **1a–3a** and **1b–3b** each show vibronic structure in their 77 K emission spectra in a rigid matrix, which indicates enhanced ³LC character at low temperature. For **1a** and **1b**, there is a small rigidochromic blueshift, which implies a CT contribution to the emission at 77 K. In contrast, the absence of any rigidochromic shift, coupled with the emission profile at room temperature for both **2b** and **3b**, compellingly points to a LC emission. The τ_e at 77 K for **1b** of 11.8 μ s is much longer than that of **1a** (4.26 μ s), **2b** (4.66 μ s), or **3b** (4.34 μ s). The presence of the methyl group in **2a** and **2b** leads to a modest enhancement of τ_e compared with **3a** and **3b**, respectively.

All six complexes are strongly luminescent in degassed ACN, however, **1b**, with a Φ_{PL} of 47%, is less bright than the other five complexes, which have Φ_{PL} values of around 75%. Complex **1b** also has the longest τ_e of the six complexes at 6.18 μ s, which contributes to the lower Φ_{PL} . There is a 7.6-fold decrease in the radiative rate constant, k_r , compared with **1a**, which is partially offset by the 2.4-fold decrease in k_{nr} . From the data previously reported for **3a,b** and our own measurements, we conclude that the methyl groups on the C^N ligands do not impact the emission energy, but modestly increase the value of k_r .^[13b,20] Complexes **1a–3a** have similar k_r values and each emits from a mixed CT state. Complexes **2b** and **3b** have similar k_r values and each emits from a predominantly LC state. The dissonant behavior of **1b** compared with **2b** (and **3b**) supports the notion that the nature of its excited state is distinct from the last two.

The dmabpy-based triplet emitters are extremely sensitive to the presence of oxygen with Φ_{PL} in aerated ACN solutions of only between 0.4–0.7%. The increased steric bulk in the presence of *tert*-butyl groups and the CT nature of the emission contribute to a decrease in the O₂-quenching sensitivity, with aerated Φ_{PL} values of 3.7–4.9%.

Electrochemistry and Electrochemoluminescence Studies

The electrochemical properties were investigated by cyclic voltammetry (CV) in ACN and the results are summa-

rized in Table 3. All electrochemical processes are either quasi-reversible or reversible at a scan rate of 100 mV/s. The oxidation process has been assigned to a largely iridium-centered event, with the potential modulated by the nature of the C^N ligands, whereas the reduction is localized on the N^N ancillary ligand (*dt*Bubpy and dmabpy at ca. –1.46 and –1.78 V, respectively). For example, **1b** underwent a quasi-reversible oxidation at 1.42 V and a reversible reduction at –1.82 V (Figure 2). Both of these potentials are significantly cathodically shifted relative to those of **1a** due to the presence of the strongly electron-donating dmabpy ligand.

Table 3. Electrochemical and electrochemoluminescence data for **1a–3a** and **1b–3b**.

	$E_{1/2,\text{ox}}$ [V] ^[a] (ΔE_p [mV])	ΔE_{redox} [V]	$E_{1/2,\text{red}}$ [V] (ΔE_p [mV])	$\Phi_{\text{ECL}}^{\text{[b]}}$ [%]	ECL λ_{max} [nm]
1a ^[c]	1.61 (100)	3.10	–1.49 (67)	17	510
1b ^[d]	1.42 (72)	3.24	–1.82 (67)	32	536
2a ^[e]	1.51 (98)	2.94	–1.42 (74)	21	533
2b	1.35 (70)	3.12	–1.77 (63)	32	510
3a	1.50 (70)	2.97	–1.47 (62)	17	519
3b	1.36 (62)	3.14	–1.78 (63)	38	527

[a] Measured in ACN (ca. 1.5 mM) with Bu₄NPF₆ (ca. 0.1 M) as the supporting electrolyte at a scan rate of 100 mV/s. The potentials were calibrated by using Fc/Fc⁺ and are reported vs. SCE. [b] Annihilation ECL efficiencies are given relative to [Ru(bpy)₃](PF₆)₂ taken as 100% in ACN (for [Ru(bpy)₃]²⁺, $\Phi_{\text{ECL}} = 0.05$).^[21] [c] ECL data taken from ref.^[5d] [d] CV data taken from ref.^[22]. [e] CV data taken from ref.^[11].

The CV profiles of **2b** and **3b** are similar to that of **1b**, but show reduced destabilization of both the oxidation and reduction reactions. We have previously shown that triazoles destabilize HOMO/LUMO orbitals in comparison with ppy-type analogues.^[11] The combined effect of *at*l and dmabpy is a further increase of 300 mV in the HOMO–LUMO gap for **1b** compared with **2a**. The electrochemical gap of 3.24 V for **1b** is larger than that recently reported for [(dFppz)₂Ir(dmabpy)]PF₆ at 3.19 V.^[17] For further comparison, the first oxidation and reduction waves for previously

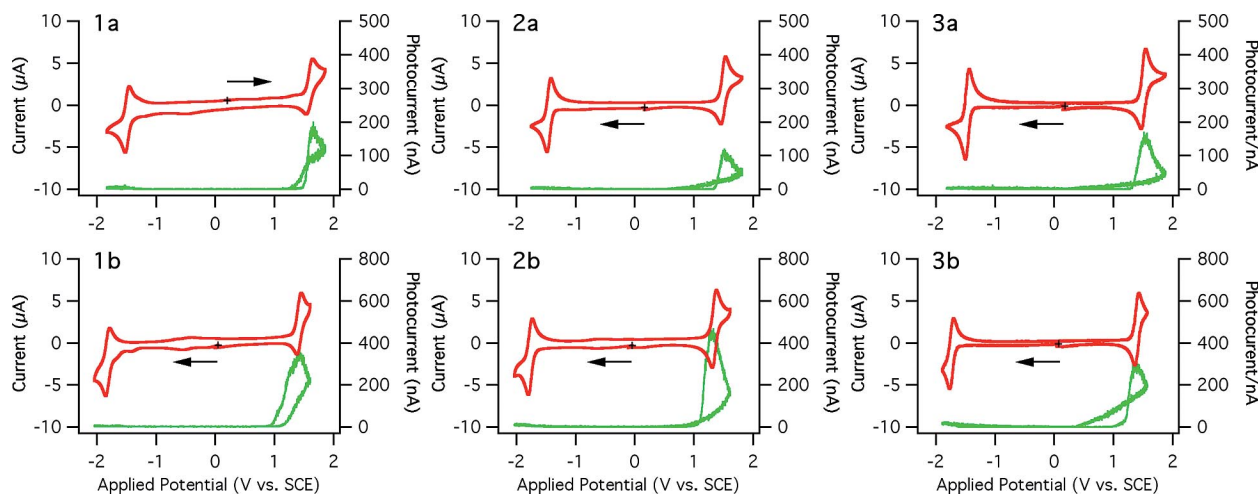


Figure 2. CV (red) with ECL–voltage curves (green) overlaid for **1a–3a** and **1b–3b**, first oxidation and reduction potential profiles at a scan rate of 0.1 V/s.

reported **3b** occur at 1.36 and -1.78 V, respectively, correlating well with those measured for **2b**. Thus, the inclusion of the methyl group does not appreciably affect the electrochemical gap.

ECL is the emission of light from excited states produced by electron transfer between radical anions and cations gen-

erated electrochemically in the vicinity of the working electrode during potential scanning/cycling in electrochemical measurements. Moderately strong ECL emission was observed from all six complexes during dynamic potential scanning (green curves in Figure 2) in the regions of the first oxidation and reduction reactions. All the ECL–volt-

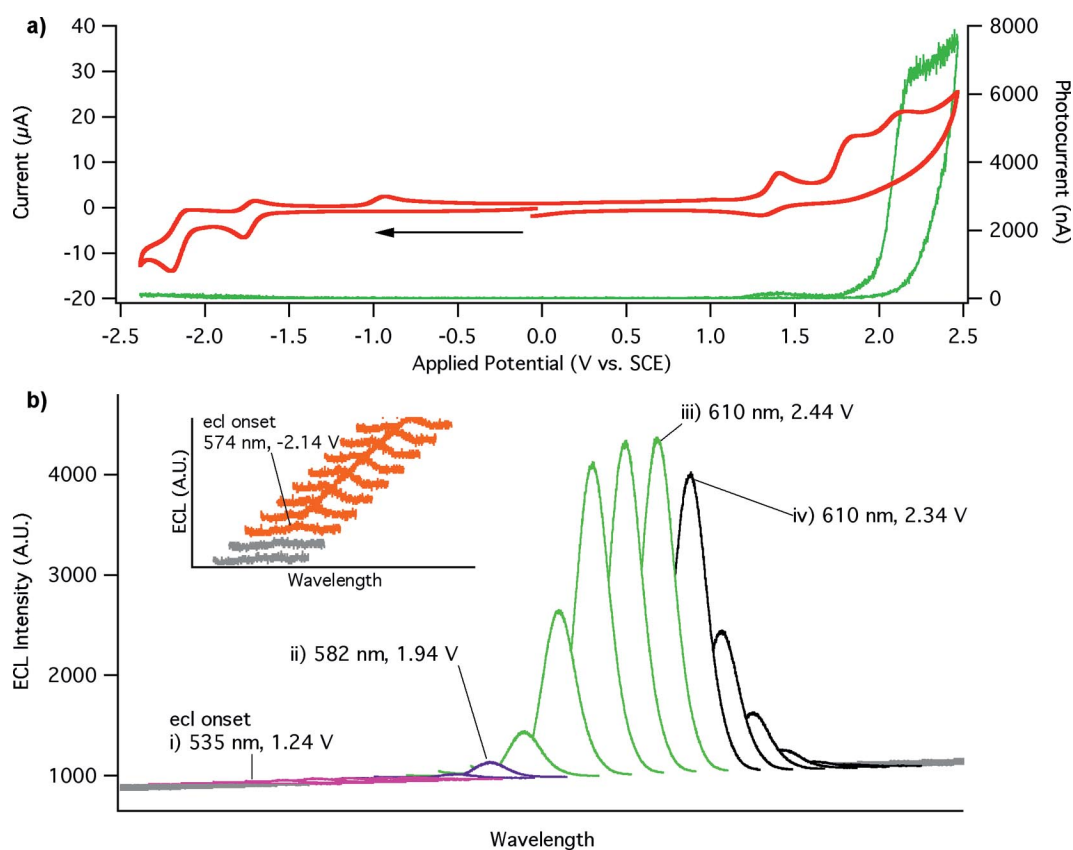


Figure 3. a) CV with ECL–voltage curve overlaid for a potential profile ranging between -2.34 and 2.44 V, b) ECL spooling spectra of **2b** during the first potential scanning cycle in the range of -2.34 to 2.44 V and at a scan rate of 0.1 V/s (each spectrum was acquired with a time interval of 1 s), showing the evolution of three wavelengths: i) the initial ECL onset, 535 nm at 1.24 V (pink), ii) 582 nm at 1.94 V (purple), iii) 610 nm at 2.44 V (green), and the devolution of one wavelength: iv) 610 nm at 2.34 V. The inset displays the ECL onset with a peak wavelength of 574 nm at -2.14 V (orange) in the second potential scanning cycle.

age curves show light emission in the anodic regions, which shows the radical anions to be more stable than the radical cations.

The ECL annihilation efficiencies were evaluated when the applied potential was scanned between the first reduction and oxidation peak potentials (Table 3). Complexes **1b–3b** generated modestly high ECL signals relative to **1a**^[5d] once the radical anions and radical cations had combined to generate the excited species (Figure 2). In fact, each of **1a–3a** exhibit low ECL efficiencies due to the presence of the two *tert*-butyl groups on the bipyridine. The Φ_{ECL} (based on two cycles) for **2b** (32%) is identical to that of **1b** (32%), whereas that of **3b** shows a higher ECL efficiency of 38%. Thus, the electron-donating character plays an important role in the ECL behavior. Each of the complexes follows the same annihilation ECL mechanism as we previously determined for **1a**,^[5d] in which triplet excited species can be generated directly from the radicals without passing through the singlet excitons.

The ECL spectra are generally redshifted with respect to the photoluminescent spectra due to the higher concentrations required during ECL acquisition and are broad and unstructured (Table 3).^[23] Although a slight redshift of 337 cm^{-1} is observed in the unstructured ECL spectrum of

1b compared with **1a**, **2b** exhibits a maximum at $\lambda_{\text{ECL}} = 510\text{ nm}$, which makes it, to the best of our knowledge, amongst the bluest ECL-active phosphors known (see Figure S10 in the Supporting Information).^[5c]

When the potential window was extended to include the second and third oxidations of **2b** (see Figures 3 and 4), a large enhancement in ECL was observed. A similar trend has previously been reported for **1b**.^[22] Initially for **2b**, the Ir center is oxidized and the onset of ECL is observed at 1.24 V, reaching a maximum of approximately 110 nA of ECL at 1.44 V. Upon scanning to more positive potentials, the two dimethylamino (dma) groups on the dmabpy ligand were each oxidized in the range of 1.94 to 2.44 V. The oxidation of the dma substituents occurs by a similar mechanism to the oxidation of tri-*n*-propylamine (TPrA), however, this route is a self-co-reactant pathway because the dma groups are part of the complex's design and not added to the solution as a typical co-reactant. When scanning to 1.94 V, the ECL increased to 580 nA because of the oxidation of the first dma group, and ECL enhancement occurs through recruitment of the generated radicals by the self-co-reactant pathway. Increasing the potential to 2.44 V results in the oxidation of the second dma substituent and results in a significant enhancement in ECL, 7880 nA. The

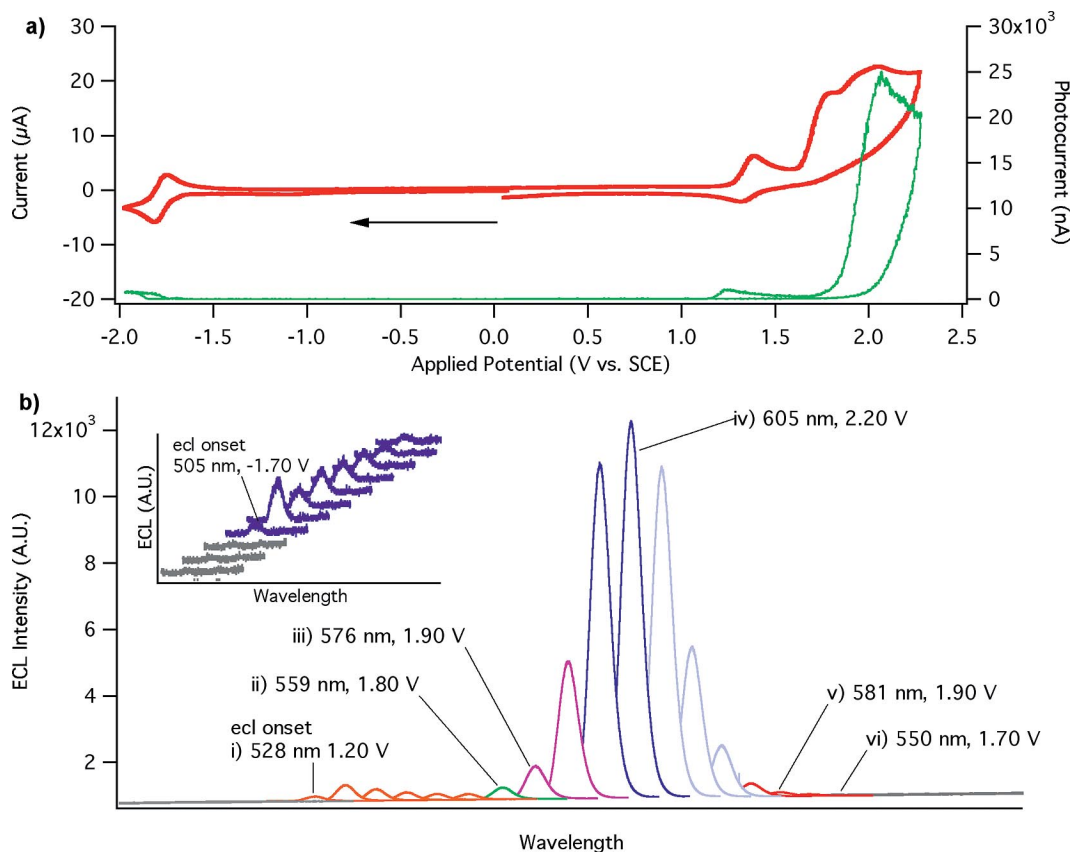
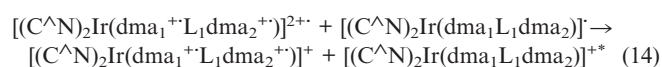
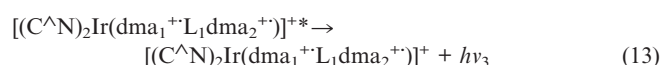
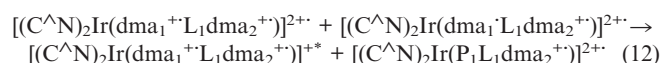
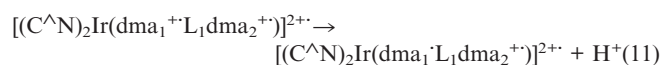
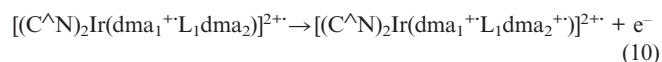
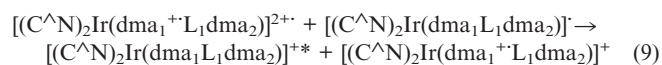
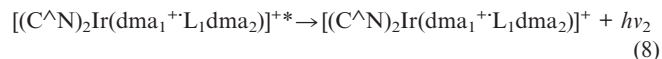
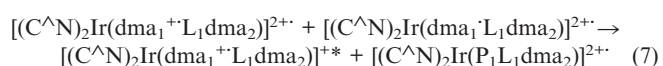
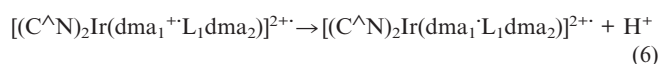
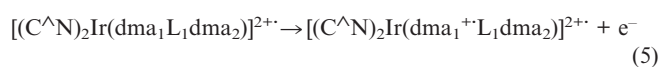
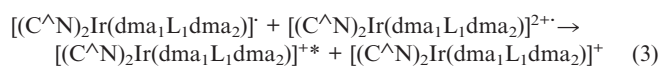
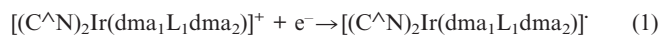


Figure 4. a) CV with ECL–voltage curve overlaid for a potential profile ranging between -2.00 and 2.30 V , b) ECL spooling spectra of **3b** during the first potential scanning cycle in the range of -2.00 to 2.30 V and at a scan rate of 0.1 V/s (each spectrum was acquired with a time interval of 1 s), showing the evolution of four wavelengths: i) initial ECL onset, 528 nm at 1.20 V (orange), ii) 559 nm at 1.80 V (green), iii) 576 nm at 1.90 V (pink), iv) 605 nm at 2.20 V (dark blue), and the devolution of three wavelengths: iv) 605 nm at 2.30 V (light blue), v) 581 nm at 1.90 V (red), vi) 550 nm at 1.70 V (dark grey). The inset displays the ECL onset with a peak wavelength of 505 nm at -1.70 V (purple) in the second potential scanning cycle.

ECL relative self-co-reactant efficiencies, Φ_{ECL} (based on one cycle), were higher when the potential window was extended and the dma substituents on the dmabpy ligand were both oxidized. An increase in efficiency is observed for **2b** (129%) and an even more dramatic enhancement for **3b** (538%). Notably, subtle changes in the structure of the complex, in this case the absence of the methyl group on the C[^]N ligands in **3b**, confers a large increase in ECL efficiency. Complex **3b** has a similar relative efficiency to **1b** (550%), however, the structure of the coordinating moiety of the C[^]N ligands differs between the pyridine in **3b** and the *N*-benzyltriazole in **1b**, with **1b** being more efficient.

To track the emission mechanisms with the extended potential window, ECL spooling spectra were collected at a time interval of 1 s with an applied potential scanning rate of 0.1 V/s for two complete cycles as in part a of Figure 3 (the potential was scanned from 0.00 to -2.34 V then to positive potentials until 2.44 V, then back to 0.00 V). Figure 3 (b) shows the ECL spectra for **2b** collected for one complete potential scanning cycle. A weak emission at 535 nm is observed at 1.24 V. The emission is redshifted to 582 nm at 1.94 V, which is caused by the change from an electron-donating dma group to an electron-withdrawing dma⁺ radical on the dmabpy ligand as we had previously concluded.^[22] The intensity of the emission continued to increase in intensity while simultaneously redshifting to 610 nm during the course of potential scanning to 2.44 V. The emission intensity began to decrease as the potential was lowered from 2.44 V back towards 0.00 V until it returned to its baseline, however, the emission remained at 610 nm.

The above observations of the self-co-reactant ECL routes can be summarized by the following four mechanisms involving the generation of an excited species with and without the dma groups acting as a TPRA-like self-co-reactant. The C[^]N ligand is dFMeppy for **2b** and dFppy for **3b**, and L₁ represents the bpy core of the ancillary ligand possessing two dma groups, dma₁ and dma₂, which together constitute the dmabpy ligand [Equations (1), (2), (3), (4), (5), (6), (7), (8), (9), (10), (11), (12), (13) and (14)], where P₁ = -(CH₃)N⁺=CH₂.



The structure of **2b**, containing the methylated pyridine fragment within its C[^]N ligand, differs from **1b**, which contains the triazole within its C[^]N ligand, however, three emissions were observed in both cases when scanning the potential to their third oxidations, and ECL thus proceeds through similar mechanisms as previously reported. Here, for **2b**, the three emissions are observed at 535 [Equation (4)], 582 [Equation (8)], and 610 nm [Equation (13)]. Interestingly, when the potential was scanned towards negative potentials in the second cycle, weak ECL emission was seen at -2.14 V, after the first reduction of **2b**, which corresponds to a wavelength of 574 nm. This onset is due to the presence of a small amount of radical cations generated in the first cycle. These radicals could react with the radical anion generated at -2.14 V, producing ECL at 574 nm.

Structurally, **3b** differs from **2b** by the removal of the methyl substituent from the pyridine unit of the C[^]N ligand. For **3b**, an apparent additional emission is observed compared with **2b** when scanning to its third oxidation (Figure 4). The four emissions are at 528 [Equation (4) via Equation (3) or Equation (9) or Equation (14)], 559, 576 [Equation (8)], and 605 nm [Equation (13)], in the spooled spectra, with a similar onset to that described for **2b**. Likewise, when the potential was scanned from 0.00 V towards negative potentials in the second cycle, at -1.70 V an additional ECL emission was observed at 505 nm. The emission at 576 nm (1.90 V) may have been the result of simultaneous detection of the emission resulting from generation of excited species following the second oxidation of **3b** at 1.80 V (559 nm) and the third oxidation of **3b** at 2.00 V (605 nm). The intensity of the emission moving from 1.20 to 2.20 V continues to increase along with a concomitant redshift of the emission. When the ECL intensity began to decrease, the emission started to blueshift back to 581 nm at 1.90 V and finally to 550 nm at 1.70 V. This shift in emission on devolution, the return scan, may be due to the dy-

namics in the vicinity of the electrode. It is important to note that scanning to the first or second reduction of the complexes did not change the peak wavelengths for the ECL emissions. Complexes **1b–3b** all show similar ECL emissions, even with different C[^]N ligands, however, the ECL intensity differs dramatically between **2b** (8.0×10^3 nA) and **3b** (2.5×10^4 nA).

Computations

To obtain a better understanding of the optoelectronic properties of **1a–3b** and to rationalize in particular the disparate photophysical behavior between **1b** and **2b**, a combined DFT and TDDFT study was undertaken in the presence of acetonitrile as solvent. Frequency calculations confirmed that energy minima had been attained in all cases. A summary of the computed optimized structural parameters of the S_0 and T_1 states for each of the six complexes can be found in Figures S11 and S12 in the Supporting Information. The Ir–N_{C[^]N}, Ir–C[^]N, and Ir–N_{N[^]N} bond lengths for triazole-containing **1a** and **1b** are on average 2.047, 2.051, and 2.163 Å respectively, which are slightly elongated compared with those in the X-ray structure of [(dFphtl)₂Ir(bpy)](PF₆) (Ir–N_{C[^]N} = 1.998 Å, Ir–C[^]N = 2.027 Å, Ir–N_{N[^]N} = 2.129 Å).^[11] The average Ir–N_{C[^]N}, Ir–C[^]N, and Ir–N_{N[^]N} bond lengths for **2a–3b** are 2.074, 2.051, and 2.177 Å, respectively, which are in good agreement with those of the X-ray structure of **2a** (Ir–N_{C[^]N} = 2.014 Å, Ir–C[^]N = 2.047 Å, Ir–N_{N[^]N} = 2.176 Å), although the calculations do predict a longer Ir–N_{C[^]N} bond. The

(C–Ir–N)_{C[^]N} and (N–Ir–N)_{N[^]N} bond angles remain constant for the six complexes with average values of 80.3 and 75.8°, respectively. A slightly more pronounced twisting of the two pyridine rings of the dmabpy ligand of 4.3 and 9.5° in both **2b** and **3b** compared with in **1b** [(N–C–N)_{dmabpy} = 0.6°] is predicted to occur, however, such a torsion is not unprecedented. Indeed, a twisted conformation of the dmabpy ligand [(N–C–N)_{dmabpy} = 15.2°] in the related [(dFppz)₂Ir(dmabpy)]PF₆ has been noted.^[17] The geometry of the triplet state of each complex generally mirrors that of the ground state although the N[^]N ligand is flattened. The principle geometric distortions in the triplet state compared with the ground state for **1b–3b** are a contraction of the Ir–N_{N[^]N} bond of around 0.04 Å, larger than the 0.02 Å contraction found for **1a–3a**.

Figure 5 compares the energy levels of selected occupied and unoccupied molecular orbitals (MOs) of the S_0 state along with the energies of the highest singly occupied MO (HSOMO) of the T_1 state. The calculated HOMO–LUMO gaps follow the trend deduced from the electrochemical data, with **1b** exhibiting the largest HOMO–LUMO and electrochemical gaps. For all the complexes, the HOMO is composed mainly of π_{C^N} and Ir t_{2g} orbitals. However, there is also a minor contribution (11–21%) in the HOMO from the dmabpy ligand in **1b–3b**, which is absent in the d/Bubpy-containing complexes. A major change is noted in the nature of the HOMO–1, in which the electron density is situated mainly on the ancillary ligand for dmabpy-containing complexes, whereas for d/Bubpy-containing complexes it is localized on the C[^]N ligand. In addition, the

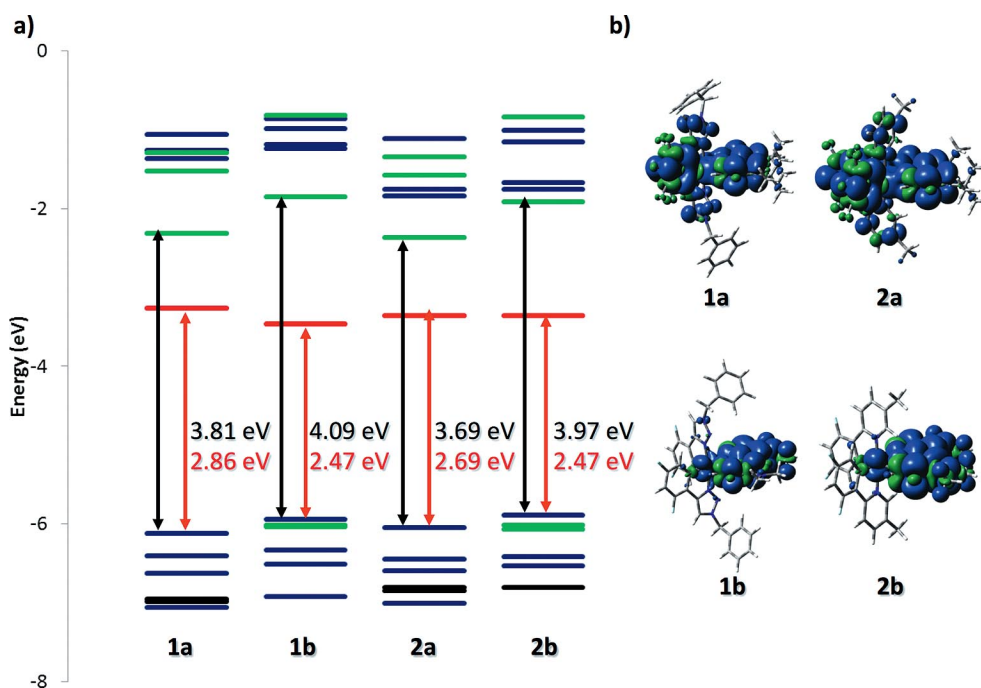


Figure 5. a) Schematic diagram of the energy values of HOMO–4 through to LUMO+5 for **1a,b** and **2a,b** obtained by DFT. Green indicates that the electron density is mostly localized on the N[^]N ligand, blue on the C[^]N ligand, and black represents a complex distribution of the electron density. The energies of the HSOMOs (red) of **1a,b** and **2a,b** were determined by unrestricted DFT of the T_1 state. b) Spin density distribution (isovalue: 0.0004 ebohr⁻³) of the T_1 state computed for **1a,b** and **2a,b**.

energy gap between the HOMO and HOMO–1 for **1b–3b** is minute, whereas this energy difference is substantially larger for **1a–3a**. The HOMO and LUMO energies of **1a–3a** are similar, and the corresponding HOMO–LUMO gaps thus vary slightly [$\sigma(\Delta E_{H-L}) = 0.06$ eV]. The HOMO and LUMO energies for **1b–3b** are destabilized compared with those of **1a–3a** due to the electron-releasing dmabpy ligand. The magnitude of the destabilization is more pronounced for the LUMO, resulting in larger HOMO–LUMO gaps, corroborating the electrochemical observations. The incorporation of the triazole moiety into **1a** and **1b** results in a slight further stabilization of the HOMO and a slight destabilization of the LUMO compared with benchmark complexes **2a**, **2b**, **3a**, and **3b**, as we have previously shown by using a lower level of theory.^[11] The LUMO is localized on the π^* orbitals of the N \wedge N moiety in each of the six complexes, a topology mirrored in the ³HSOMO. The topology of the LUMO+1 in **1a** is also predominantly N \wedge N, whereas in **1b–3b** the electron density is localized on the C \wedge N ligands. Compared with the LUMO, the LUMO+1 orbitals in **2b** and **3b** are only slightly further destabilized by 0.16 and 0.21 eV, respectively, whereas in the case of **1b**, the LUMO–LUMO+1 energy gap is larger at 0.61 eV. The tight clustering of MOs in **2b** and **3b** results in a mixing of the electronic transitions involved. Remarkably, although the HOMO–LUMO gap increases with the incorporation of the dmabpy ligand, the HOMO–HSOMO gap actually decreases significantly in energy. The complexes with *d*/Bubpy ligands have a calculated LUMO–HSOMO gap of around 1.0 eV. This energy gap is much larger for the dmabpy series (1.62, 1.50, and 1.54 eV for **1b**, **2b**, and **3b**, respectively). The larger value calculated for **1b** explains the lack of blueshift in its emission.

The important low-energy singlet–singlet transitions along with the five lowest-energy singlet–triplet transitions computed by using the TDDFT approach at the same level of theory are presented in Table 4. The TDDFT computations accurately predict the principal bands observed in the absorption spectra (see Figures S13–S18 in the Supporting Information). In all cases, the HOMO→LUMO transition is extremely weak and is ¹MLCT and ¹LLCT in nature. For **1b**, the dominant low-energy transition at 345 nm is absent in the *d*/Bubpy family of complexes. This HOMO–1→LUMO transition (*S*₂ state) is ¹LC_{N \wedge N} in nature with some ¹ILCT_{N \wedge N} character. The *S*₈ and *S*₁₀ states are ¹LLCT in nature with the charge transfer unusually from the N \wedge N to the C \wedge N ligands. Likewise, this same behavior is evident in **2b**, in which the *S*₄ state is a mixture of ¹LC_{N \wedge N} and ¹ILCT_{N \wedge N} transitions and the *S*₈ state is mainly ¹LLCT_{N \wedge N→C \wedge N}. Complex **2b** distinguishes itself from **1b** by showing increased ¹LC character due to contributions from the *S*₂ and *S*₄ states. These intense ¹LC transitions at around 350 nm are observed only with the dmabpy family of complexes (see Figures S14, S16, and S18).

To investigate the nature of the phosphorescence, the five lowest-energy singlet–triplet transitions for **1a**, **1b**, and **2b** were calculated for the optimized ground-state geometries by using a TDDFT approach. The *T*₁ state for **1a**, which

resides 3.12 eV above the *S*₀ state, is composed of a HOMO→LUMO transition and implies a mixed MLCT and LLCT character in the emission. The unpaired-electron spin density distribution for **1a** agrees perfectly with this assignment (Figure 5, b). Analogously, **2a** and **3a** show emission with similar CT character. For **1b**, the first two triplet states *T*₁ and *T*₂ are nearly isoenergetic and are 2.94 and 2.97 eV above the ground state, respectively. The *T*₁ state is best described as having ³LC_{dmabpy} character but with additional important ³MLCT and ³LLCT character. The *T*₂ state, which is composed mainly of a HOMO–1→LUMO transition, is a mixed ³LC_{dmabpy}/³MLCT. The large ³LC_{dmabpy} character is reflected in the spin density distribution for **1b**, which is localized principally on the dmabpy ligand and the iridium atom. The origin of the ³LC character results from the fact that the HOMO–1 and HOMO–2 orbitals lie within 0.1 eV of the HOMO, and the HOMO–2→LUMO (65%) and HOMO–1→LUMO (90%) transitions are responsible for the *T*₁ and *T*₂ states, respectively. The *T*₃–*T*₅ states are of similar energy at 3.38, 3.41, and 3.41 eV, respectively. They are each characterized by a series of vertical transitions, defined by ³LC_{C \wedge N} character. Similarly to **1b**, the first four triplet states for **2b** are very close in energy, ranging from 2.90 to 2.97 eV. The first two triplet states, composed of HOMO–2→LUMO (62%) and HOMO→LUMO (29%), and HOMO–1→LUMO (89%), respectively, are mainly ³LC_{dmabpy} in character with some ³MLCT and ³LLCT. The *T*₃ and *T*₄ states are characterized each by a series of transitions with ³LC_{dFMep_{py}} character. The *T*₅ state (3.33 eV) is mainly ³LLCT_{C \wedge N→N \wedge N} with some ³MLCT/³LLCT due to the predominance of the HOMO→LUMO (57%) transition. The four nearly isoenergetic triple states in **2b**, each with significant ³LC character, contribute to an enhancement of the LC emission compared with **1b**. The increased ³LC character in the emission of **2b** and **3b** compared with **1b** results from the smaller separation in energy of the LUMO (dmabpy-centered) and LUMO+1 (C \wedge N ligand-centered) for these two complexes. Thus, ³LC_{C \wedge N} emission occurs from HOMO→LUMO+1 and HOMO→LUMO+2 transitions in addition to ³LC_{N \wedge N}. Thus, the use of *d*Fphtl as a C \wedge N ligand promotes emission that has increased CT character than *d*FMep_{py} due to a larger destabilization of the π^* orbitals in the former.

The emission energies were calculated by three distinct approaches in acetonitrile solution (Table 5). The energy difference between the *T*₁ and *S*₀ states in their respective optimized geometries is an effective approximation to the *E*_{0,0} experimental values measured at low temperature. The predictions agree well with experiment with the relative errors not exceeding 4.2%. The emission energies predicted by TDDFT (*S*₀→*T*₁) for the optimized *S*₀ geometry are on average blueshifted by 20 nm compared with the computed *E*_{0,0} values due to 1) the closed-shell nature of the calculation and 2) the neglect of geometric relaxation of the *T*₁ state. Theoretical adiabatic electronic emission, *E*_{A_E}, calculated as the vertical energy difference between the *T*₁ and *S*₀ states in the optimized *T*₁ geometry, correlate reasonably well with the emission maxima at 298 K.

Table 4. Lowest-energy singlet and triplet excited states for **1a**, **1b**, and **2b**.^[a]

	State	λ [nm]	E [eV]	Assignment [f]	Nature
1a	S ₁	394	3.15	H→L (98%) [0.0004]	¹ LLCT _{C[^]N→N[^]N/¹MLCT}
	S ₂	348	3.57	H-1→L (97%) [0.0357]	¹ LLCT _{C[^]N→N[^]N/¹MLCT}
	S ₆	312	3.98	H-4→L (77%) [0.1747]	¹ LLCT _{C[^]N→N[^]N/¹MLCT}
	T ₁	397.4	3.12	H→L (90%)	³ MLCT/ ³ LLCT
	T ₂	387.0	3.20	H-10→L (41%), H-3→L (23%)	³ MLCT/ ³ LLCT/LC _{dmabpy}
	T ₃	368.0	3.37	H-1→L+2 (16%), H→L+2 (29%)	³ LC _{dFphtl}
	T ₄	363.7	3.41	H-1→L+4 (16%), H→L+4 (20%)	³ LC _{dFphtl}
	T ₅	357.5	3.47	H-4→L (17%), H-1→L (55%)	³ MLCT/ ³ LLCT
1b	S ₁	359	3.45	H→L (96%) [0.0015]	¹ LLCT _{C[^]N→N[^]N/¹MLCT}
	S ₂	345	3.59	H-1→L (97%) [0.2554]	¹ LC _{N[^]N/¹ILCT_{N[^]N/¹MLCT}}
	S ₈	300	4.13	H-1→L+1 (89%) [0.0204]	¹ LLCT _{N[^]N→C[^]N/¹MLCT}
	S ₁₀	295	4.21	H-2→L+1 (63%) [0.0848]	¹ LLCT _{N[^]N→C[^]N/¹MLCT}
	T ₁	421.7	2.94	H-2→L (65%), H→L (27%)	³ LC _{dmabpy} / ³ MLCT/ ³ LLCT
	T ₂	417.2	2.97	H-1→L (90%)	³ LC _{dmabpy} / ³ MLCT
	T ₃	366.4	3.38	H-3→L+2 (12%), H-3→L+4 (14%), H→L+1 (26%), H→L+3 (15%)	³ ILCT _{dFphtl} / ³ LC _{dFphtl}
	T ₄	363.9	3.41	H-3→L+1 (15%), H-3→L+3 (18%), H→L+2 (19%), H→L+4 (14%)	³ ILCT _{dFphtl} / ³ LC _{dFphtl}
	T ₅	363.5	3.41	H-10→L (30%), H-8→L (12%), H-6→L (14%), H-2→L+5 (12%), H-1→L+6 (11%)	³ LC _{dFphtl}
	2b	S ₁	374	3.31	H→L (87%) [0.0034]
S ₂		369	3.36	H→L+1 (84%) [0.0787]	¹ LC _{C[^]N/¹ILCT_{C[^]N/¹MLCT}}
S ₄		353	3.51	H-1→L (91%) [0.2724]	¹ LC _{N[^]N/¹ILCT_{N[^]N/¹MLCT}}
S ₈		333	3.73	H-1→L+2 (49%)	¹ LLCT _{N[^]N→C[^]N/¹MLCT}
T ₁		427.1	2.90	H-2→L+1 (46%) [0.1309] H-2→L (62%), H→L (29%)	³ LC _{dmabpy} / ³ MLCT/ ³ LLCT
T ₂		423.2	2.93	H-1→L (89%)	³ LC _{dmabpy} / ³ MLCT/ ³ LLCT
T ₃		421.4	2.94	H-4→L+1 (11%), H-3→L+2 (21%), H→L+1 (49%)	³ LC _{dFMeppy}
T ₄		417.7	2.97	H-4→L+2 (11%), H-3→L+1 (28%), H→L+2 (38%)	³ LC _{dFMeppy}
T ₅		372.2	3.33	H-2→L (27%), H→L (57%)	³ MLCT/ ³ LLCT/ ³ LC _{dmabpy}

[a] Singlet–singlet and singlet–triplet transitions computed by TDDFT (see text for details) with dominant monoexcitations of >10% (contribution in parentheses) along with the description of the nature of the excited state. H = HOMO; L = LUMO, f = oscillator strength in brackets; f for singlet–triplet transitions is 0.

From these predictions several conclusions can be drawn. Substitution of the pyridine ring with a triazole results in a blueshift of the emission spectrum (**1a** vs. **2a** and **3a** and **1b** vs. **3b**), which has been verified computationally ($E_{0,0}$ values). The impact of the methyl group on the pyridine of the C[^]N ligand is less conclusive. Experimentally, there is a slight redshift in the 77 K emission in **2a** and **2b** compared with in **3a** and **3b**, respectively. Computationally, a small blueshift in the $E_{0,0}$ emission of 18 nm for **2b** compared

with **3b** is predicted, whereas a redshift of 5 nm is predicted for **2a** compared with **3a**. The absence of a further blueshift for **1b**, **2b**, and **3b** compared with **1a** resides in the fact that although the dmabpy ligand significantly destabilizes the LUMO (and somewhat less the HOMO), this destabilization is not translated onto the triplet manifold and the energy of ³HSOMO is only modestly affected (Figure 4), resulting in only a meager impact on the phosphorescence energy ($E_{0,0}$) between **1a** and **1b**, **2b**, or **3b**.

Table 5. Predicted phosphorescence energies for **1a–3a** and **1b–3b** employing different approaches.

	Theoretical ^[a]				Experimental ^[b]		
	λ_{TDDFT} [nm]	$\lambda_{0,0}$ [nm]	λ_{AE} [nm]	$\lambda_{\text{em}}(77\text{ K})$ [nm]	Error ^[c] [%]	$\lambda_{\text{em}}(298\text{ K})$ [nm]	Error ^[d] [%]
1a	397.4	415.5	459.0	433	4.2	498	8.5
1b	421.7	457.9	496.5	459	0.3	495	0.3
2a	419.1	437.4	484.1	456	4.2	512	5.8
2b	427.1	444.2	488.6	459	3.3	494	1.1
3a	414.2	432.3	478.0	448	3.6	519	8.6
3b	431.6	462.0	521.1	454	1.7	490	6.0

[a] λ_{TDDFT} = wavelength of $S_0 \rightarrow T_1$ transition obtained by TDDFT at the S_0 optimized geometry. $\lambda_{0,0} = 1240/[E(T_1) - E(S_0)]$ at their respective optimized geometries obtained by DFT. $\lambda_{\text{AE}} = 1240/[E(T_1) - E(S_0)]$ at the T_1 optimized geometry (adiabatic electronic emission) obtained by DFT. See Exp. Sect. for computational details. All values were determined with ACN as solvent. [b] Highest-energy emission band at 77 K reported and highest-intensity emission band at 298 K reported. [c] Error = $[(E_{\text{em}}(77\text{ K}) - E_{0,0})/E_{\text{em}}(77\text{ K})] \times 100$ in %; the emission energies are in eV. [d] Error = $[(E_{\text{em}}(298\text{ K}) - E_{\text{AE}})/E_{\text{em}}(298\text{ K})] \times 100$ in %; the emission energies are in eV.

Conclusions

Two new highly luminescent cationic blue-emitting iridium complexes (**1b** and **2b**) are reported and fully characterized. The combination of dFphtl and dmabpy ligands was chosen to shift the emission maximum further to the blue than in the case of **1a**, which has a less electron-releasing *t*Bu group on the ancillary ligand. The absence of a larger blueshift in the emission of **1b** ($\lambda_{\text{max}} = 498$ nm) is due to the poor sensitivity of the triplet-state energy upon change of the ancillary ligand from d/Bubpy to dmabpy. The presence of the dFphtl C[^]N ligand in **1b** promotes emission from the ^3LC state with considerable $^3\text{MLCT}$ and $^3\text{LLCT}$ character at 298 K, inferred from the structureless emission, solvatochromism, and computations. In contrast, the structured and solvent-invariant emission observed at 298 K for **2b** and **3b** coupled with the computations point to emission from both $^3\text{LC}_{\text{C}^{\wedge}\text{N}}$ and $^3\text{LC}_{\text{N}^{\wedge}\text{N}}$ states. The redox behavior of the six complexes is similar in that each has a quasi-reversible oxidation wave and a reversible reduction wave. The presence/absence of the methyl group does not alter the nature of the emission. Introduction of the dFphtl ligand shifts the oxidation anodically but the reduction cathodically whereas the incorporation of the electron-donating NMe₂ group shifts both the oxidation and reduction cathodically, resulting in a large electrochemical gap of 3.24 V for **1b** compared with 3.12 V for **2b**. These complexes are ECL-active under annihilation conditions, emitting sky-blue to blue-green light. Complexes bearing d/Bubpy N[^]N ligands are less bright than their dmabpy congeners in the ECL spectra. Upon scanning to 2.50 V, dramatic enhancement in the ECL emission was observed. The absence of the methyl group in **3b** leads to an enhancement in the ECL signal of 538%, whereas for **2b**, the ECL signal is only enhanced by 129%. This study illustrates the inherent difficulties and challenges in designing 1) highly efficient cationic blue emitters and the limitations in pushing the emission further to the blue by using π -acceptor ancillary ligands and 2) developing highly efficient ECL luminophores. We are nevertheless currently evaluating these luminophores both in the solid state for LEEC devices and in solution as ECL-based biological probes.

Experimental Section

General Procedures: Commercial chemicals were used as supplied. 1-Benzyl-4-(2,4-difluorophenyl)-1*H*-1,2,3-triazole (dFphtl) was prepared following a one-pot protocol previously developed by us,^[24] 2-(2,4-difluorophenyl)-5-methylpyridine (dFMeppyH) was obtained by Kröhnke condensation,^[25] and 2-(2,4-difluorophenyl)pyridine (dFppyH) was obtained by Suzuki coupling between 2-bromopyridine and 1-bromo-2,4-difluorobenzene. 4,4'-Bis(dimethylamino)-2,2'-bipyridine (dmabpy) was synthesized from 2,2'-bipyridine in 12% overall yield over five steps according to a procedure adapted from the literature.^[15] Complexes **1a–3a** and **3b** were prepared according to the literature.^[11]

All reactions were performed by using standard Schlenk techniques under N₂, save for the click reactions. Flash column chromatography was performed by using silica gel (Silia-P from Silicycle, 60 Å, 40–63 μm). Analytical TLC was performed by using silica plates with aluminium backings (250 μm with indicator F-254). Compounds were visualized under UV light. ¹H and ¹³C NMR spectra were recorded with either a Bruker Avance spectrometer at 400 and 100 MHz, respectively, or a Bruker Avance spectrometer at 300 and 75 MHz, respectively. The following abbreviations have been used for multiplicity assignments: “s” for singlet, “d” for doublet, “t” for triplet, “m” for multiplet, and “br.” for broad. Deuteriated acetonitrile (CD₃CN) was used as the solvent except where noted below. Spectra were referenced to the solvent peak. Melting points were recorded by using open-end capillaries on a Meltemp melting point apparatus. Accurate mass measurements were performed with a quadrupole time-of-flight (ES-Q-TOF) spectrometer, model Synapt MS G1 from Waters in positive electrospray mode, and spectra were recorded at the Université de Sherbrooke.

[(dFphtl)₂Ir(dmabpy)](PF₆) (1b**):** Complex **1b** was obtained by first isolating the μ -dichloro-bridged iridium(III) dimer described by Nonoyama.^[16] The cleavage of the dimer (323 mg, 0.21 mmol, 0.50 equiv.) was accomplished by addition of dmabpy (101 mg, 0.42 mmol, 1.00 equiv.) in ethylene glycol (7 mL). The suspension was degassed by successive cycles of vacuum and N₂ purging and finally heated at 150 °C for 18 h. The clear orange solution was cooled to room temperature, diluted with water (75 mL), and the resulting aqueous phase was then extracted with Et₂O. The aqueous phase was heated at 60 °C for 15 min, cooled to room temperature, and an aqueous solution of NH₄PF₆ (10 mL, 1.0 g/10 mL) was added dropwise to the aqueous phase to cause precipitation of a yellow solid. The suspension was cooled to 0 °C for 1 h, filtered,

and the resulting solid was washed with cold water. The resulting solid was purified by flash chromatography on silica gel by using a gradient of DCM and acetone (from 100% DCM to 95:5 DCM/acetone). The purified complex was redissolved in a minimum amount of MeOH and precipitated again by its addition to an NH_4PF_6 solution (1.0 mL; 1 g/10 mL). The solid complex was filtered, washed with water, and dried under vacuum to yield a yellow powder (220 mg, 47%), m.p. 104 °C (dec.). $R_f = 0.32$ (alumina; DCM/acetone, 9:1). ^1H NMR (300 MHz, CD_3CN): $\delta = 8.15$ (s, 2 H), 7.48–7.30 (m, 10 H), 7.18 (dd, $J = 7.1, 2.1$ Hz, 4 H), 6.61 (td, $J = 10.0, 2.2$ Hz, 2 H), 6.52 (dd, $J = 6.7, 2.7$ Hz, 2 H), 5.77 (dd, $J = 9.1, 2.2$ Hz, 2 H), 5.52 (s, 4 H), 3.15 (s, 12 H) ppm. ^{13}C NMR (75 MHz, CD_3CN): $\delta = 165.6$ (d, $J = 10.9$ Hz), 162.3 (d, $J = 10.9$ Hz), 160.0 (d, $J = 13.0$ Hz), 157.6 (s), 156.7 (d, $J = 13.0$ Hz), 156.0 (s), 153.6 (d, $J = 5.5$ Hz), 150.4 (s), 135.6 (s), 130.0 (s), 129.8 (s), 128.6 (s), 122.5 (d, $J = 5.5$ Hz), 115.8 (dd, $J = 17.8, 2.4$ Hz), 109.5 (s), 106.1 (s), 98.2 (dd, $J = 27.4, 23.8$ Hz), 56.2 (s), 40.0 (s) ppm. LRMS (ES-Q-TOF): $m/z = 973$ $[\text{M}]^+$. HR-MS [ES-Q-TOF]: calcd. for $[\text{C}_{44}\text{H}_{38}\text{F}_4\text{N}_{10}\text{Ir}]^+$ 973.2823; found 973.2804.

[(dFMeppy)₂Ir(dmabpy)](PF₆) (2b): dFMeppyH (173 mg, 0.84 mmol, 2.00 equiv.) was mixed with iridium trichloride (127 mg, 0.43 mmol, 1.00 equiv.) in a mixture of 2-ethoxyethanol and water (12 mL, 5:1). The mixture was degassed by multiple vacuum and N_2 purging cycles and the suspension was heated at 150 °C for 18 h. A yellow precipitate formed. To this reaction mixture was added dmabpy (106 mg, 0.44 mmol, 1.02 equiv.) and the suspension was left at 150 °C for a further 18 h. The reaction mixture was cooled to room temperature and diluted with water (75 mL). The aqueous suspension was extracted with Et_2O and the aqueous layer was heated at 60 °C for 15 min and cooled to room temperature. A solution of NH_4PF_6 (10 mL, 1.0 g/10 mL) was added dropwise to the aqueous phase to cause precipitation of a yellow solid. The suspension was cooled to 0 °C for 1 h, filtered, and the resulting solid was washed with cold water. The resulting solid was purified by flash chromatography on silica gel by using DCM as eluent. The purified complex was redissolved in a minimum amount of MeOH and precipitated again by its addition to an NH_4PF_6 solution (1.0 mL; 1 g/10 mL). The solid complex was filtered, washed with water, and dried under vacuum to yield a yellow powder (117 mg, 27%), m.p. 171 °C (dec.). $R_f = 0.11$ (silica; DCM). ^1H NMR (300 MHz, CD_3CN): $\delta = 8.20$ (d, $J = 8.4$ Hz, 2 H), 7.73 (d, $J = 8.6$ Hz, 2 H), 7.54 (s, 2 H), 7.47 (d, $J = 2.6$ Hz, 2 H), 7.37 (d, $J = 6.7$ Hz, 2 H), 6.68–6.52 (m, 4 H), 5.75 (dd, $J = 8.7, 2.2$ Hz, 2 H), 3.15 (s, 12 H), 2.17 (s, 6 H) ppm. ^{13}C NMR (75 MHz, CD_3CN): $\delta = 170.2$ (d, $J = 13$ Hz), 168.0 (d, $J = 15$ Hz), 166.8 (d, $J = 9.7$ Hz), 164.5 (d, $J = 13$ Hz), 161.8 (d, $J = 4.7$ Hz), 161.0 (s), 160.4 (s), 153.9 (s), 144.9 (s), 139.3 (s), 133.4 (s), 128.1 (d, $J = 20$ Hz), 118.9 (d, $J = 17.1$ Hz), 114.6 (s), 111.3 (s), 103.0 (t, $J = 27$ Hz), 44.3 (s), 22.6 (s) ppm. LRMS (ES-Q-TOF): 841 $[\text{M}]^+$. HRMS (ES-Q-TOF): calcd. for $[\text{C}_{38}\text{H}_{34}\text{F}_4\text{N}_6\text{Ir}]^+$ 841.2387; found 841.2410.

Photophysical Characterization: All samples were prepared in either HPLC-grade acetonitrile (ACN) or a mixture of spectroscopic-grade methanol (MeOH) and ethanol (EtOH) with concentrations in the order of 25 μM . Absorption spectra were recorded at room temperature in a 1.0 cm capped quartz cuvette using a Shimadzu UV-1800 double beam spectrophotometer. Molar absorptivity determination was verified by a linear least-squares fit of values obtained from at least four independent solutions at varying concentrations with absorptions ranging from (0.01–1.6 a.u.). Emission spectra were recorded at both room temp. and at 77 K in 1.0 cm septa-sealed quartz cells from Starna and NMR tubes, respectively. Steady-state emission spectra were obtained by exciting at the long-

est wavelength absorption maxima and using a Horiba Jobin Yvon Fluorolog-3 spectrofluorimeter equipped with double monochromators and a photomultiplier tube detector (Hamamatsu model R955). Emission quantum yields were determined by using the optically dilute method.^[26] A stock solution for each complex with an absorbance of around 0.5 was prepared and then four dilutions were obtained with dilution factors of 40, 20, 13.3, and 10 resulting in optical dilution absorbances of around 0.013, 0.025, 0.038, and 0.05, respectively. The Beer–Lambert law was assumed to remain linear at the concentrations of the solutions. The emission spectra were then measured after the solutions had been rigorously degassed with solvent-saturated N_2 for 20 min prior to spectrum acquisition. For each sample, linearity between absorption and emission intensity was verified through linear regression analysis and additional measurements were acquired until the Pearson regression factor (R_2) for the linear fit of the data set surpassed 0.9. Individual relative quantum yields were calculated for each solution and the values reported represent the slope obtained from the linear fit of these results. The equation $\Phi_s = \Phi_r(A_r/A_s)(I_s/I_r)(n_r/n_s)^2$ was used to calculate the relative quantum yield of a sample in which Φ_r is the absolute quantum yield of the reference, n is the refractive index of the solvent, A is the absorbance at the excitation wavelength, and I is the integrated area under the corrected emission curve. The subscripts s and r refer to the sample and reference, respectively. A solution of $[\text{Ru}(\text{bpy})_3](\text{PF}_6)_2$ in ACN was used as the external reference ($\Phi_r = 0.095$ and 0.018, respectively, for deaerated and aerated measurements)^[19]. The experimental uncertainty in the emission quantum yields is conservatively estimated to be 10%, although we have found that statistically we can reproduce PLQYs to within 3% relative error.

Time-resolved excited-state lifetime measurements were determined by using the time-correlated single photon counting (TCSPC) option of the Jobin Yvon Fluorolog-3 spectrofluorimeter. A pulsed NanoLED at 341 nm, (pulse duration <1 ns; fwhm = 14 nm), mounted directly on the sample chamber at 90° to the emission monochromator, was used to excite the samples and photons were collected by using a FluoroHub single-photon-counting detector from Horiba Jobin Yvon. The luminescence lifetimes were obtained by using the commercially available Horiba Jobin Yvon Decay Analysis Software (version 6.4.1) included within the spectrofluorimeter. Lifetimes were determined by an assessment of the goodness of its mono- or biexponential fit by minimizing the chi-squared function (χ^2) and by visual inspection of the weighted residuals.

Electrochemistry and Electrogenerated Chemiluminescence Characterization: For annihilation ECL studies, approximately 2 mg of compound (**1a–3a** and **1b–3b**) was added to a Pyrex electrochemical cell with a flat Pyrex window at the bottom for detection of generated ECL. A 2 mm diameter Pt disc inlaid in a glass sheath was used as the working electrode (WE), a coiled Pt wire as the counter electrode (CE), and a coiled Ag wire as the quasi-reference electrode (RE). Routine cleaning procedures for the electrodes and cell are reported elsewhere.^[5d,27] For detailed electrochemical workstation and ECL setup information, please refer to our previous publications.^[5d,27] The cell contained 0.1 M tetrabutylammonium hexafluorophosphate (TBAPF₆) as the supporting electrolyte in anhydrous acetonitrile (3 mL) and was assembled in a dry box.

Cyclic voltammetry (CV) was performed with a CHI 610A electrochemical analyzer (CH Instruments, Austin, TX). The experimental parameters for the cyclic voltammograms (CVs) are as follows: 0.00 V initial potential on the experimental scale, positive or negative initial scan polarity, 0.1 V/s scan rate, 4 sweep segments,

0.001 V sample interval, 2 s quiet time, $(1-5) \times 10^{-5} \text{ A V}^{-1}$ sensitivity. Potentials were calibrated by using an internal standard Fc/Fc^+ redox couple after each experiment and are reported versus a SCE standard electrode (0.40 V in ACN).^[28]

The ECL data along with CV data were obtained by using the CHI 610A instrument coupled with a photomultiplier tube (PMT, R928, Hamamatsu, Japan) maintained at -750 V with a high voltage power supply. The ECL collected by the PMT under the flat Pyrex window at the bottom of the cell was measured as a photocurrent and transformed to a voltage signal by using a picoammeter/voltage source (Keithley 6487, Cleveland, OH). The potential, current signals from the electrochemical workstation, and the photocurrent signal from the picoammeter were sent simultaneously through a DAQ board (DAQ 6052E, National Instruments, Austin, TX) in a computer. The data acquisition system was controlled from a custom-made LabVIEW program (ECL_PMT610a.vi, National Instruments, Austin, TX). The photosensitivity of the picoammeter was set manually to avoid saturation.

The ECL spectra were obtained by replacing the PMT with a spectrometer (Cornerstone 260, Newport, Canada) attached to a CCD camera (Model DV420-BV, Andor Technology, Belfast, UK). The camera was cooled to $-55 \text{ }^\circ\text{C}$ prior to use and controlled by a computer for operation and data acquisition. The intensities versus wavelengths (spectra) were recorded by using Andor SOLIS (version 4.19.30001.0, see ref.^[22]) from Andor Technology.

ECL quantum efficiencies (QE) were calculated relative to $[\text{Ru}(\text{bpy})_3](\text{PF}_6)_2$ taken as 100% in acetonitrile solution (absolute quantum ECL efficiency of $[\text{Ru}(\text{bpy})_3]^{2+}$ is 0.05^[29]) by integrating both the ECL intensity and current value versus time for each compound, as described in Equation (15),

$$\Phi_x = 100 \times \left(\frac{\int_a^b \text{ECL } dt}{\int_a^b \text{Current } dt} \right)_x \bigg/ \left(\frac{\int_a^b \text{ECL } dt}{\int_a^b \text{Current } dt} \right)_{st} \quad (15)$$

in which x represents the compounds **1a–3b**, a and b represent the integral time range, and st represents $[\text{Ru}(\text{bpy})_3](\text{PF}_6)_2$.

For the spooling experiments, the same spectrometer and CCD camera were used and the following parameters were employed in the Andor Technology program under the kinetic parameters option tab. For **2b**, exposure time = 1 s, number of accumulations = 1, kinetic series length = 175 s (matching with the potential scan time for two complete cycles), kinetic cycle time = 1, and the spectrometer was centered at 500 nm by using the 121.6 lines per mm grating, with the camera cooled to $-55 \text{ }^\circ\text{C}$. On the CHI 610A electrochemical analyzer, the initial potential was set to 0.00 V, high potential = 2.44 V, low potential = -2.34 V , sensitivity = $1 \times 10^{-5} \text{ A V}^{-1}$, initial scan polarity = negative, scan rate = 0.1 V/s sweep segments = 4, sample interval = 0.001 V, quiet time 2 s. The CHI 610A electrochemical analyzer and the Andor Technology program were run simultaneously and the CV data and spooling spectra were collected. For **3b**, exposure time = 1 s, number of accumulations = 1, kinetic series length = 155 s (matching with the potential scan time for two complete cycles), kinetic cycle time = 1, and the spectrometer was centered at 600 nm by using the 121.6 lines per mm grating, with the camera cooled to $-55 \text{ }^\circ\text{C}$. On the CHI 610A electrochemical analyzer, the initial potential was set to 0.00 V, high potential = 2.20 V, low potential = -2.00 V , sensitivity = $1 \times 10^{-5} \text{ A V}^{-1}$, initial scan polarity = negative, scan rate = 0.1 V/s, sweep segments = 4, sample interval = 0.001 V, quiet time

2 s. The CHI 610A electrochemical analyzer and the Andor Technology program were run simultaneously and the CV and spooling spectra were collected.

Density Functional Theory (DFT) Calculations: DFT calculations were performed with Gaussian 09.^[30] DFT^[31] and TDDFT^[32] calculations were carried out by using the B3LYP method; excited-state triplet geometries were calculated by using the unrestricted B3LYP method (UB3LYP) with a spin multiplicity of 3.^[33] The 6-31G* basis set^[34] was used for C, H, and N directly linked to the iridium atom, the 3-21G* basis set^[35] was used for the other C, H, N, and F atoms, and the VDZ (valence double ζ) with the SBKJC effective core potential basis set^[35a,36] was used for iridium. Geometry optimizations were conducted without symmetry constraints. Frequency calculations performed on each optimized structure resulted in only positive vibrational frequencies. The phosphorescence wavelengths were predicted by energy differences between the triplet and singlet optimized states at their respective optimized geometries ($E_{0,0}$)^[10,37] and also as the energy difference between the triplet and singlet optimized states at the optimized geometry the triplet state (E_{AE}). The energy, oscillator strength, and related MO contributions for the 100 lowest singlet–singlet and 5 lowest singlet–triplet excitations were obtained from the TD-DFT/singlets and the TD-DFT/triplets output files, respectively, for the S_0 -optimized geometry. The calculated absorption spectra were obtained and visualized with GaussSum 2.1 (fwhm: 1000 cm^{-1}).^[38] All calculations were performed in acetonitrile solution by use of the polarized continuum (PCM) solvation model as implemented in Gaussian 09.^[39] This computational methodology has been demonstrated by us to provide accurate modeling of both the ground- and excited-state properties of iridium(III) complexes.^[11,40]

Supporting Information (see footnote on the first page of this article): Detailed synthetic procedures and characterization data for **1b–3b**, ^1H and ^{13}C NMR spectra for **1b–3b**, detailed photophysical, electrochemiluminescence, and computational protocols, supplementary photophysical characterization data and electrochemiluminescence spectra for **1b–3b**, computational output, including selected structural parameters, MO quantifications, UV/Vis spectra predictions, ground- and excited-state dipole moment predictions, Jablonski diagrams, and full TDDFT singlet output for **1b** and **2b**.

Acknowledgments

E. Z.-C. and Z. D. acknowledge the Canadian Foundation for Innovation (CFI), the National Sciences and Engineering Research Council of Canada (NSERC), Le Fonds Québécois de la Recherche sur la Nature et les Technologies (FQRNT) for financial support. S. L. acknowledges the FQRNT for a Ph. D. scholarship. The authors are grateful to Ahmed Moez Soliman for help with the preparation of the dmabpy ligand and to Dr. Martina Sandroni for the preparation of additional **2b** and **3b**.

- [1] a) J. D. Slinker, J. Rivnay, J. S. Moskowitz, J. B. Parker, S. Bernhard, H. D. Abruña, G. G. Malliaras, *J. Mater. Chem.* **2007**, *17*, 2976; b) T. Hu, L. He, L. Duan, Y. Qiu, *J. Mater. Chem.* **2012**, *22*, 4206; c) S. Ladouceur, E. Zysman-Colman, *Eur. J. Inorg. Chem.* **2013**, 2985.
- [2] a) K. K.-W. Lo, S. P.-Y. Li, K. Y. Zhang, *New J. Chem.* **2011**, *35*, 265; b) Q. Zhao, F. Li, C. Huang, *Chem. Soc. Rev.* **2010**, *39*, 3007.
- [3] a) L. Hu, G. Xu, *Chem. Soc. Rev.* **2010**, *39*, 3275; b) L. Xu, Y. Li, S. Wu, X. Liu, B. Su, *Angew. Chem.* **2012**, *124*, 8192; *Angew. Chem. Int. Ed.* **2012**, *51*, 8068.

- [4] a) D. Bruce, M. M. Richter, *Anal. Chem.* **2002**, *74*, 1340; b) C. Cole, B. D. Muegge, M. M. Richter, *Anal. Chem.* **2003**, *75*, 601; c) B. D. Muegge, M. M. Richter, *Anal. Chem.* **2003**, *76*, 73; d) S. Zanarini, E. Rampazzo, S. Bonacchi, R. Juris, M. Marcaccio, M. Montalti, F. Paolucci, L. Prodi, *J. Am. Chem. Soc.* **2009**, *131*, 14208; e) J. I. Kim, I.-S. Shin, H. Kim, J.-K. Lee, *J. Am. Chem. Soc.* **2005**, *127*, 1614; f) A. Kapturkiewicz, G. Angulo, *Dalton Trans.* **2003**, 3907; g) A. Kapturkiewicz, J. Nowacki, P. Borowicz, *Electrochim. Acta* **2005**, *50*, 3395; h) A. Kapturkiewicz, T.-M. Chen, I. R. Laskar, J. Nowacki, *Electrochim. Commun.* **2004**, *6*, 827; i) C. Li, J. Lin, X. Yang, J. Wan, *J. Organomet. Chem.* **2011**, *696*, 2445; j) I.-S. Shin, J. I. Kim, T.-H. Kwon, J.-I. Hong, J.-K. Lee, H. Kim, *J. Phys. Chem. C* **2007**, *111*, 2280; k) I.-S. Shin, S. Yoon, J. I. Kim, J.-K. Lee, T. H. Kim, H. Kim, *Electrochim. Acta* **2011**, *56*, 6219; l) J. Roop, M. Nothnagel, M. Schnuriger, M. M. Richter, G. A. Baker, *J. Electroanal. Chem.* **2011**, *656*, 34; m) I.-S. Shin, Y.-T. Kang, J.-K. Lee, H. Kim, T. H. Kim, J. S. Kim, *Analyst* **2011**, *136*, 2151; n) E. H. Doeven, E. M. Zammit, G. J. Barbante, C. F. Hogan, N. W. Barnett, P. S. Francis, *Angew. Chem.* **2012**, *124*, 4430; *Angew. Chem. Int. Ed.* **2012**, *51*, 4354.
- [5] a) M. Bandini, M. Bianchi, G. Valenti, F. Piccinelli, F. Paolucci, M. Monari, A. Umani-Ronchi, M. Marcaccio, *Inorg. Chem.* **2010**, *49*, 1439; b) H. Lin, M. E. Cinar, M. Schmittel, *Dalton Trans.* **2010**, *39*, 5130; c) S. Zanarini, M. Felici, G. Valenti, M. Marcaccio, L. Prodi, S. Bonacchi, P. Contreras-Carballada, R. M. Williams, M. C. Feiters, R. J. M. Nolte, L. De Cola, F. Paolucci, *Chem. Eur. J.* **2011**, *17*, 4640; d) K. N. Swanick, S. Ladouceur, E. Zysman-Colman, Z. Ding, *Chem. Commun.* **2012**, *48*, 3179; e) M.-J. Li, P. Jiao, M. Lin, W. He, G.-N. Chen, X. Chen, *Analyst* **2011**, *136*, 205; f) C. Li, J. Lin, Y. Guo, S. Zhang, *Chem. Commun.* **2011**, *47*, 4442; g) R. V. Kiran, C. F. Hogan, B. D. James, D. J. D. Wilson, *Eur. J. Inorg. Chem.* **2011**, 4816; h) Q. Shu, L. Birkenbach, M. Schmittel, *Inorg. Chem.* **2012**, *51*, 13123.
- [6] a) M. Schmittel, Q. Shu, M. E. Cinar, *Dalton Trans.* **2012**, *41*, 6064; b) M. Schmittel, S. Qinghai, *Chem. Commun.* **2012**, *48*, 2707.
- [7] B. D. Muegge, M. M. Richter, *Luminescence* **2005**, *20*, 76.
- [8] S. O. Jeon, J. Y. Lee, *J. Mater. Chem.* **2012**, *22*, 7239.
- [9] a) L. He, L. Duan, J. Qiao, R. Wang, P. Wei, L. Wang, Y. Qiu, *Adv. Funct. Mater.* **2008**, *18*, 2123; b) L. He, J. Qiao, L. Duan, G. Dong, D. Zhang, L. Wang, Y. Qiu, *Adv. Funct. Mater.* **2009**, *19*, 2950; c) M. Mydlak, C. Bizzarri, D. Hartmann, W. Sarfert, G. Schmid, L. De Cola, *Adv. Funct. Mater.* **2010**, *20*, 1812; d) L. He, L. Duan, J. Qiao, D. Zhang, L. Wang, Y. Qiu, *Chem. Commun.* **2011**, *47*, 6467; e) M. Felici, P. Contreras-Carballada, Y. Vida, J. M. M. Smits, R. J. M. Nolte, L. De Cola, R. M. Williams, M. C. Feiters, *Chem. Eur. J.* **2009**, *15*, 13124; f) L. He, L. Duan, J. Qiao, G. Dong, L. Wang, Y. Qiu, *Chem. Mater.* **2010**, *22*, 3535; g) A. B. Tamayo, S. Garon, T. Sajoto, P. I. Djurovich, I. M. Tsyba, R. Bau, M. E. Thompson, *Inorg. Chem.* **2005**, *44*, 8723; h) C.-H. Yang, J. Beltran, V. Lemaux, J. Cornil, D. Hartmann, W. Sarfert, R. Fröhlich, C. Bizzarri, L. De Cola, *Inorg. Chem.* **2010**, *49*, 9891; i) C. Shik Chin, M.-S. Eum, S.-y. Kim, C. Kim, S. Kwon Kang, *Eur. J. Inorg. Chem.* **2007**, 372; j) H.-F. Chen, W.-Y. Hung, S.-W. Chen, T.-C. Wang, S.-W. Lin, S.-H. Chou, C.-T. Liao, H.-C. Su, H.-A. Pan, P.-T. Chou, Y.-H. Liu, K.-T. Wong, *Inorg. Chem.* **2012**, *51*, 12114; k) S. B. Meier, W. Sarfert, J. M. Junquera-Hernandez, M. Delgado, D. Tordera, E. Orti, H. J. Bolink, F. Kessler, R. Scopelliti, M. Gratzel, M. K. Nazeeruddin, E. Baranoff, *J. Mater. Chem.* **2013**, *1*, 58.
- [10] M. S. Lowry, W. R. Hudson, R. A. Pascal Jr., S. Bernhard, *J. Am. Chem. Soc.* **2004**, *126*, 14129.
- [11] S. Ladouceur, D. Fortin, E. Zysman-Colman, *Inorg. Chem.* **2011**, *50*, 11514.
- [12] a) J. M. Fernández-Hernández, C.-H. Yang, J. I. Beltrán, V. Lemaux, F. Polo, R. Fröhlich, J. Cornil, L. De Cola, *J. Am. Chem. Soc.* **2011**, *133*, 10543; b) M. Felici, P. Contreras-Carballada, J. M. M. Smits, R. J. M. Nolte, R. M. Williams, L. De Cola, M. C. Feiters, *Molecules* **2010**, *15*, 2039; c) S. Liu, P. Müller, M. K. Takase, T. M. Swager, *Inorg. Chem.* **2011**, *50*, 7598; d) B. Beyer, C. Ulbricht, D. Escudero, C. Friebe, A. Winter, L. González, U. S. Schubert, *Organometallics* **2009**, *28*, 5478.
- [13] a) M. K. Nazeeruddin, R. T. Weng, Z. Zhou, C. Klein, Q. Wang, F. DeAngelis, S. Fantacci, M. Grätzel, *Inorg. Chem.* **2006**, *45*, 9245; b) F. De Angelis, S. Fantacci, N. Evans, C. Klein, S. M. Zakeeruddin, J.-E. Moser, K. Kalyanasundaram, H. J. Bolink, M. Gratzel, M. K. Nazeeruddin, *Inorg. Chem.* **2007**, *46*, 5989.
- [14] H. J. Bolink, E. Coronado, R. n. D. Costa, N. Lardiés, E. Orti, *Inorg. Chem.* **2008**, *47*, 9149.
- [15] D. Zhang, J. P. Telo, C. Liao, S. E. Hightower, E. L. Clennan, *J. Phys. Chem. A* **2007**, *111*, 13567.
- [16] M. Nonoyama, *Bull. Chem. Soc. Jpn.* **1974**, *47*, 767.
- [17] E. Baranoff, H. J. Bolink, E. C. Constable, M. Delgado, D. Haussinger, C. E. Housecroft, M. K. Nazeeruddin, M. Neuberger, E. Orti, G. E. Schneider, D. Tordera, R. M. Walliser, J. A. Zampese, *Dalton Trans.* **2013**, *42*, 1073.
- [18] W. H. Melhuish, *J. Phys. Chem.* **1961**, *65*, 229.
- [19] H. Ishida, S. Tobita, Y. Hasegawa, R. Katoh, K. Nozaki, *Coord. Chem. Rev.* **2010**, *254*, 2449.
- [20] a) The previously reported Φ_{PL} for **3b** was 85% in ACN ($\lambda_{\text{em}} = 463$ and 493 nm, $\tau_{\text{e}} = 4.11 \mu\text{s}$) with a k_{nr} of $0.4 \times 10^5 \text{ s}^{-1}$ (see ref.^[13b]). In our hands, the Φ_{PL} for **3b** was found to be 73% in ACN ($\lambda_{\text{em}} = 464$ and 490 nm, $\tau_{\text{e}} = 3.69 \mu\text{s}$), essentially identical to that of **2b**; b) Bolink and co-workers (ref.^[14]) reported the 298 K emission for **3a** at 512 nm with a Φ_{PL} of 70% and a τ_{e} of 1.4 μs , whereas we measured a Φ_{PL} of 78% and a τ_{e} of 1.35 μs .
- [21] a) P. McCord, A. J. Bard, *J. Electroanal. Chem.* **1991**, *318*, 91; b) J. E. Bartelt, S. M. Drew, R. M. Wightman, *J. Electrochem. Soc.* **1992**, *139*, 70.
- [22] K. N. Swanick, S. Ladouceur, E. Zysman-Colman, Z. Ding, *Angew. Chem. Int. Ed.* **2012**, *51*, 11079.
- [23] R. Y. Lai, A. J. Bard, *J. Phys. Chem. B* **2003**, *107*, 5036.
- [24] S. Ladouceur, A. M. Soliman, E. Zysman-Colman, *Synthesis* **2011**, 3604.
- [25] F. Kröhnke, *Synthesis* **1976**, 1.
- [26] G. A. Crosby, J. N. Demas, *J. Phys. Chem.* **1971**, *75*, 991.
- [27] a) C. Booker, X. Wang, S. Haroun, J. Zhou, M. Jennings, B. L. Pagenkopf, Z. Ding, *Angew. Chem.* **2008**, *120*, 7845; *Angew. Chem. Int. Ed.* **2008**, *47*, 7731; b) K. N. Swanick, D. W. Dodd, J. T. Price, A. L. Brazeau, N. D. Jones, R. H. E. Hudson, Z. Ding, *Phys. Chem. Chem. Phys.* **2011**, *13*, 17405.
- [28] N. G. Connelly, W. E. Geiger, *Chem. Rev.* **1996**, *96*, 877.
- [29] a) P. McCord, A. J. Bard, *J. Electroanal. Chem.* **1991**, *318*, 91; b) J. E. Bartelt, S. M. Drew, R. M. Wightman, *J. Electrochem. Soc.* **1992**, *139*, 70.
- [30] M. J. Frisch, G. W. Trucks, H. B. Schlegel, G. E. Scuseria, M. A. Robb, J. R. Cheeseman, G. Scalmani, V. Barone, B. Mennucci, G. A. Petersson, H. Nakatsuji, M. Caricato, X. Li, H. P. Hratchian, A. F. Izmaylov, J. Bloino, G. Zheng, J. L. Sonnenberg, M. Hada, M. Ehara, K. Toyota, R. Fukuda, J. Hasegawa, M. Ishida, T. Nakajima, Y. Honda, O. Kitao, H. Nakai, T. Vreven, J. A. Montgomery, J. E. Peralta, F. Ogliaro, M. Bearpark, J. J. Heyd, E. Brothers, K. N. Kudin, V. N. Staroverov, R. Kobayashi, J. Normand, K. Raghavachari, A. Rendell, J. C. Burant, S. S. Iyengar, J. Tomasi, M. Cossi, N. Rega, J. M. Millam, M. Klene, J. E. Knox, J. B. Cross, V. Bakken, C. Adamo, J. Jaramillo, R. Gomperts, R. E. Stratmann, O. Yazyev, A. J. Austin, R. Cammi, C. Pomelli, J. W. Ochterski, R. L. Martin, K. Morokuma, V. G. Zakrzewski, G. A. Voth, P. Salvador, J. J. Dannenberg, S. Dapprich, A. D. Daniels, Ö. Farkas, J. B. Foresman, J. V. Ortiz, J. Cioslowski, D. J. Fox, *Gaussian 09*, revision 7.0, Gaussian, Inc., Wallingford, CT, **2009**.
- [31] a) P. Hohenberg, W. Kohn, *Phys. Rev. B* **1964**, *136*, 864; b) W. Kohn, L. Sham, *J. Phys. Rev. A* **1965**, *140*, 1133; c) D. R. Salahub, M. C. Zerner (Eds.), *The Challenge of d and f Electrons*,

- ACS, Washington, DC, **1989**; d) R. G. Parr, W. Yang, *Density-functional theory of atoms and molecules*, Oxford University Press, Oxford, UK, **1989**.
- [32] a) R. E. Stratmann, G. E. Scuseria, M. J. Frisch, *J. Chem. Phys.* **1998**, *109*, 8218; b) R. Bauernschmitt, R. Ahlrichs, *Chem. Phys. Lett.* **1996**, *256*, 454; c) M. E. Casida, C. Jamorski, K. C. Casida, D. R. Salahub, *J. Chem. Phys.* **1998**, *108*, 4439.
- [33] a) A. D. Becke, *J. Chem. Phys.* **1993**, *98*, 5648; b) C. Lee, W. Yang, R. G. Parr, *Phys. Rev. B* **1988**, *37*, 785; c) B. Miehlich, A. Savin, H. Stoll, H. Preuss, *Chem. Phys. Lett.* **1989**, *157*, 200.
- [34] V. A. Rassolov, J. A. Pople, M. A. Ratner, T. L. Windus, *J. Chem. Phys.* **1998**, *109*, 1223.
- [35] a) J. S. Binkley, J. A. Pople, W. J. Hehre, *J. Am. Chem. Soc.* **1980**, *102*, 939; b) M. S. Gordon, J. S. Binkley, J. A. Pople, W. J. Pietro, W. J. Hehre, *J. Am. Chem. Soc.* **1982**, *104*, 2797; c) W. J. Pietro, M. M. Francl, W. J. Hehre, D. J. Defrees, J. A. Pople, J. S. Binkley, *J. Am. Chem. Soc.* **1982**, *104*, 5039; d) K. D. Dobbs, W. J. Hehre, *J. Comput. Chem.* **1986**, *7*, 359; e) K. D. Dobbs, W. J. Hehre, *J. Comput. Chem.* **1987**, *8*, 861; f) K. D. Dobbs, W. J. Hehre, *J. Comput. Chem.* **1987**, *8*, 880.
- [36] a) W. J. Stevens, W. J. Basch, M. Krauss, *J. Chem. Phys.* **1984**, *81*, 6026; b) W. J. Stevens, M. Krauss, H. Basch, P. G. Jasien, *Can. J. Chem.* **1992**, *70*, 612; c) T. R. Cundari, W. J. Stevens, *J. Chem. Phys.* **1993**, *98*, 5555.
- [37] S. Ladouceur, D. Fortin, E. Zysman-Colman, *Inorg. Chem.* **2010**, *49*, 5625.
- [38] N. M. O'Boyle, *GaussSum 2.0*, Dublin City University, Dublin, **2006**, available at <http://gausssum.sf.net>.
- [39] a) S. Miertuš, E. Scrocco, J. Tomasi, *Chem. Phys.* **1981**, *55*, 117; b) J. Tomasi, B. Mennucci, R. Cammi, *Chem. Rev.* **2005**, *105*, 2999.
- [40] a) K. Hasan, E. Zysman-Colman, *Inorg. Chem.* **2012**, *51*, 12560; b) L. Donato, P. Abel, E. Zysman-Colman, *Dalton Trans.* **2013**, *42*, 8402; c) A. M. Soliman, D. Fortin, P. D. Harvey, E. Zysman-Colman, *Dalton Trans.* **2012**, *41*, 9382.

Received: July 4, 2013

Published Online: ■

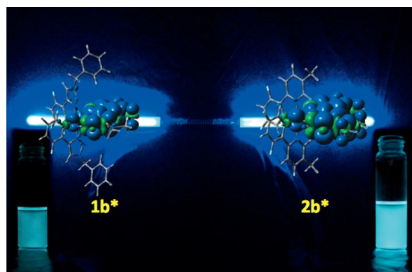
Luminescent Iridium Complexes

S. Ladouceur, K. N. Swanick,
S. Gallagher-Duval, Z. Ding,*
E. Zysman-Colman* 1–16



Strongly Blue Luminescent Cationic Iridium(III) Complexes with an Electron-Rich Ancillary Ligand: Evaluation of Their Optoelectronic and Electrochemiluminescence Properties

Keywords: Iridium / Electrochemistry / Nitrogen heterocycles / UV/Vis spectroscopy / Electrochemiluminescence / Density functional calculations



The synthesis, photophysical, electrochemical, and electrochemiluminescent properties of two highly emissive cationic blue-emitting Ir complexes are reported. Variation of the ligand results in a change in the nature of the emission. The decoration on both the cyclometalating and ancillary ligands strongly influences the ECL efficiencies. A detailed DFT/TDDFT study corroborates experiment.